Distributed Extended Object Tracking with Adaptive Networks

Kaidi Yang*, Wei Xia*†, Mengqing Zhou‡
* School of Information and Communication Engineering,
University of Electronic Science and Technology of China, Chengdu 611731, China
E-mail: kdy@std.uestc.edu.cn, wx@uestc.edu.cn, zhoumq0202@163.com
† School of Computer Science and Technology (School of Cyberspace Security), Xinjiang University, Ürümqi 830046, China.
‡ Novasky Technology Company Limited by Shares, Changsha 410221, China.

***Abstract*—In this work, we consider tracking an elliptical extended object with adaptive networks. We propose a distributed extended object tracking algorithm for adaptive networks based on the diffusion strategy. The simulation results validate the superior performance as well as the computational efficiency of the proposed DEOT algorithm for adaptive networks.**

I. Introduction

Target tracking is pivotal for applications such as navigation, surveillance, etc [1]. Conventional target tracking generally retrieves only the kinematic state, namely, position, velocity, acceleration, of an object, neglecting its extension (e.g., orientation, size and shape). With the increasing sensor resolution capabilities, extended object tracking (EOT), which retrieves both the kinematic and extension of either object or group target, has recently been arising increasing attention [2]–[4].

Approaches based on different models, such as hypersurface and elliptic shape, etc., have recently been successfully applied to EOT [2], [5]. The elliptical shape model is chosen herein owing to its compactness and mathematical convenience in representing the extent of an object with a few parameters, thereby enabling efficient Bayesian inference with relatively low computational cost [3], [4].

Distributed tracking algorithms based on adaptive networks [6], [7] have recently been gaining increasing attention due to their enhanced scalability [7]. Among various distributed strategies such as consensus [8] and incremental [9], the diffusion strategy has been shown to exhibit superior performance and robustness [10].

More recently, preliminary studies have also demonstrated that the distributed EOT algorithms based on adaptive networks can achieve preferable tracking accuracy [11], [12]. Specifically, in the distributed tracking algorithm (DRM) [11] based on the random matrix model [13], the intermediate estimates of the kinematic state and extension at each node would be effectively combined with those at its neighbors, leveraging the weighted Kullback-Leibler average scheme. Alternatively, based on the multiplicative error model and diffusion strategy, the estimate of the kinematic state and extension at each node would be updated via collaboration with its neighbors with sequentially iterating measurements. With the Gaussian Wasserstein distance (GWD) [3] as the comprehensive tracking performance metric, incorporating both the estimation errors of kinematic and extension state, the efficacy of the distributed EOT Kalman filter (DEOKF) [12] therein has been experimentally validated.

It is noteworthy that the performance of the DRM algorithm [11] would remarkably degrade in tracking object during turns owing to the fact that it would not explicitly distinguish between the uncertainty of the orientation and the semi-axes of the elliptical object, as experimentally demonstrated hereinafter. On the other hand, we would also demonstrate that the DEOKF algorithm [12] could effectively track an object during turns at the cost of computational burden, especially in scenarios with denser measurements.

In this work, we propose a computationally efficient, distributed extended object tracking (DEOT) algorithm based on the diffusion strategy with adaptive networks. Specifically, we improve computational efficiency by designing the algorithm to simultaneously process multiple measurements at each node. The simulation results validate the superior performance as well as the computational efficiency of the proposed DEOT algorithm for adaptive networks.

II. Problem Formulation

A. Dynamic Model

Similar to [5], [8], [11]–[14], we consider approximating the shape of the extended object with an ellipse. Without loss of generality, at each time instant i, the kinematic state $\boldsymbol{x}_i \triangleq [\boldsymbol{\rho}_i^{\mathrm{T}},\ \dot{\boldsymbol{\rho}}_i^{\mathrm{T}}]^{\mathrm{T}} \in \mathbb{R}^{4\times 1}$ incorporating the position $\boldsymbol{\rho}_i$ and the velocity $\dot{\boldsymbol{\rho}}_i$ of the ellipse center.

We utilize the shape parameter vector $\boldsymbol{e}_i = [a_{1,i}, a_{2,i}, \theta_i]^{\mathrm{T}} \in \mathbb{R}^{3\times 1}$ to describe the elliptical-shaped extended object at each time instant i, where $a_{1,i}$, $a_{2,i}$, and θ_i represent the semi-major and semi-minor axes, as well as the orientation of the elliptical object, respectively, as illustrated in Fig. 1. On the other hand, the extension of the elliptical object can also be characterized by a symmetric positive definite (SPD) random matrix (i.e., extension matrix) [11], [14]–[16]

$$\boldsymbol{S}_i \triangleq \boldsymbol{\Omega}_i \boldsymbol{L}_i^2 \boldsymbol{\Omega}_i^{\mathrm{T}}, \tag{1}$$

†This work was supported in part by the National Natural Science Foundation of China under Grants 62471107, 62461053. (*Corresponding author: W. Xia.*)

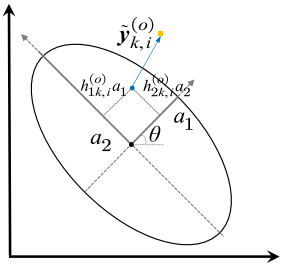

Fig. 1. Measurement model

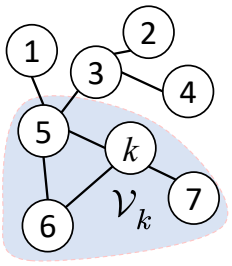

Fig. 2. Topology

with

$$\boldsymbol{\Omega}_i = \begin{bmatrix} \cos(\theta_i) & -\sin(\theta_i) \\ \sin(\theta_i) & \cos(\theta_i) \end{bmatrix}, \quad \boldsymbol{L}_i = \begin{bmatrix} a_{1,i} & 0 \\ 0 & a_{2,i} \end{bmatrix}, \tag{2}$$

respectively represent the rotation matrix and the diagonal matrix of the elliptical semi-axes.

We consider the state transition equations [5], [12], [17]

$$\boldsymbol{x}_{i+1} = \boldsymbol{F}_i^{\mathrm{x}} \boldsymbol{x}_i + \boldsymbol{w}_i^{\mathrm{x}}, \quad \boldsymbol{e}_{i+1} = \boldsymbol{F}_i^{\mathrm{e}} \boldsymbol{e}_i + \boldsymbol{w}_i^{\mathrm{e}}, \tag{3}$$

where $\boldsymbol{F}_i^{\mathrm{x}}$ and $\boldsymbol{F}_i^{\mathrm{e}}$ represent the process matrices of the kinematic state and extension state at time instant i, respectively. The process noises $\boldsymbol{w}_i^{\mathrm{x}}$ and $\boldsymbol{w}_i^{\mathrm{e}}$ are assumed to be uncorrelated, zero-mean, and white, with the priori known covariance matrices $\boldsymbol{Q}_i^{\mathrm{x}}$ and $\boldsymbol{Q}_i^{\mathrm{e}}$, respectively.

B. Measurement Model

Consider an adaptive network with N nodes in $\mathbb{R}^2$ dimensional space. The nodes are referred to as the neighbors if they could communicate directly with one another [10], [18], [19]. The set of neighbors (i.e., neighborhood, see Fig. 2) of each node k, including itself, is denoted as $\mathcal{N}_k$, with the degree $d_k \triangleq |\mathcal{N}_k|$ denoting the number of neighbors of each node k.

At each time instant i, each node k in the network is assumed to independently obtain $n_{k,i}$ uncorrelated measurements originating from these scattering sources [3], [4], [12]

$$\mathcal{Y}_{k,i} = \left[\boldsymbol{y}_{k,i}^{(1)}, \ \boldsymbol{y}_{k,i}^{(2)}, \ \ldots, \ \boldsymbol{y}_{k,i}^{(n_{k,i})} \right], \tag{4}$$

and each node k would exchange the measurements with its neighbors $l_1, l_2, \ldots, l_{d_k} \in \mathcal{V}_k$, and the measurements available at each node k at each time instant i are

$$\mathcal{Z}_{k,i} \triangleq \left[\mathcal{Y}_{l_1,i}, \mathcal{Y}_{l_2,i}, \ldots, \mathcal{Y}_{l_{d_k},i} \right] = \left[\boldsymbol{z}_{k,i}^{(1)}, \boldsymbol{z}_{k,i}^{(2)}, \ldots, \boldsymbol{z}_{k,i}^{(b_{k,i})} \right], \tag{5}$$

where $\boldsymbol{z}_{k,i}^{(\iota)}$ is the ιth column of $\mathcal{Z}_{k,i}$, and $b_{k,i} \triangleq \sum_{l \in \mathcal{V}_k} n_{l,i}$ is the total number of measurements within $\mathcal{V}_k$.

The local measurement from the ιth scattering source at each node k, denoted by $\boldsymbol{y}_{k,i}^{(\iota)}$, is modeled as

$$\boldsymbol{y}_{k,i}^{(\iota)} = \boldsymbol{H} \boldsymbol{x}_i + \boldsymbol{\Omega}_i \boldsymbol{L}_i \boldsymbol{h}_{k,i}^{(\iota)} + \boldsymbol{v}_{k,i}^{(\iota)}, \tag{6}$$

where

$$\boldsymbol{H} = [\boldsymbol{I}_2 \quad \boldsymbol{O}_2] \tag{7}$$

is the measurement matrix picking the EO position $\boldsymbol{\rho}_i$ out of the kinematic state $\boldsymbol{x}_i$, and the multiplicative noise vector $\boldsymbol{h}_{k,i}^{(\iota)} \triangleq [h_{1k,i}^{(\iota)}, h_{2k,i}^{(\iota)}]^{\mathrm{T}}$ describes the spread of the scattering sources on the surface of the extended object.

In light of [5], [12], we assume that $\boldsymbol{h}_{k,i}^{(\iota)}$ is zero-mean Gaussian white with the covariance matrix $\boldsymbol{Q}^{\mathrm{h}} = \omega \boldsymbol{I}_2$, where the scalar $\omega = 1/4$ generally indicates that the scattering sources are uniformly distributed on the elliptical surface [5], [20]. Each entry of $\boldsymbol{h}_{k,i}^{(\iota)}$ is assumed to be independent of the kinematic state $\boldsymbol{x}_i$, the matrix $\boldsymbol{\Omega}_i \boldsymbol{L}_i$, and the additive noise $\boldsymbol{v}_{k,i}^{(\iota)}$ [5]. The noise $\boldsymbol{h}_{k,i}^{(\iota)}$ at each node k is also assumed to be independent of those of other nodes [12]. In addition, following [21], we consider the potentially time-varying, distance-aware covariance matrix $\boldsymbol{R}_{k,i} = \xi \|\boldsymbol{p}_k - \boldsymbol{\rho}_i\|^2 \boldsymbol{I}_4$ of the zero-mean Gaussian additive noise $\boldsymbol{v}_{k,i}^{(\iota)}$, where $\xi > 0$ is a small positive constant, and $\boldsymbol{p}_k$ denotes the position of node k.

III. ALGORITHM DERIVATION

We develop herein a distributed extended object tracking algorithm in an adaptive network. First, the intermediate estimates of the object kinematic state and parameter vector using the measurements within its neighborhood could be attained through localized adaptation. Second, intermediate estimates shared by its neighboring nodes would be aggregated by the combination module, enabling refinement of the local estimates. Finally, the kinematic and extension states at the next time instant would be predicted by the time-update module.

A. Localized Adaption

We consider herein the localized adaptation for each node k. We use $\hat{\boldsymbol{x}}_{k,i|j}$ and $\hat{\boldsymbol{e}}_{k,i|j}$ to denote the instantaneous local estimates of the kinematic state $\boldsymbol{x}_i$ and extension state $\boldsymbol{e}_i$, respectively, obtained at each node k based on the measurements up to time instant j. We also define the state estimation error covariance matrices $\boldsymbol{P}_{k,i|j} \triangleq \mathbb{E}\left\{(\boldsymbol{x}_i - \hat{\boldsymbol{x}}_{k,i|j})(\boldsymbol{x}_i - \hat{\boldsymbol{x}}_{k,i|j})^{\mathrm{T}}\right\}$ and $\boldsymbol{B}_{k,i|j} \triangleq \mathbb{E}\left\{(\boldsymbol{e}_i - \hat{\boldsymbol{e}}_{k,i|j})(\boldsymbol{e}_i - \hat{\boldsymbol{e}}_{k,i|j})^{\mathrm{T}}\right\}$. In light of the decoupling assumption between the kinematic and the extension states [5], [12], the localized adaptation of kinematic and extension states can be derived independently.

1) Kinematic State: Akin to [11], [13], [16], [17], [20], we consider that each node would utilize the measurement average $\bar{\boldsymbol{z}}_{k,i} = \frac{1}{b_{k,i}} \sum_{\iota=1}^{b_{k,i}} \boldsymbol{z}_{k,i}^{(\iota)}$. The intermediate estimate $\boldsymbol{\psi}_{k,i}$ of the object kinematic state and the estimate $\hat{\boldsymbol{P}}_{k,i|i}$ of $\boldsymbol{P}_{k,i|i}$ could be obtained, each node k via the Kalman filter, namely,

$$\boldsymbol{\psi}_{k,i} \leftarrow \hat{\boldsymbol{x}}_{k,i|i-1}, \tag{8}$$

$$\boldsymbol{P}_{k,i} \leftarrow \boldsymbol{P}_{k,i|i-1}, \tag{9}$$

$$\boldsymbol{R}_{\mathrm{x}} \leftarrow \boldsymbol{H} \boldsymbol{P}_{k,i} \boldsymbol{H}^{\mathrm{T}} + (\omega b_{k,i} \hat{\boldsymbol{\Omega}}_i \hat{\boldsymbol{L}}_i^2 \hat{\boldsymbol{\Omega}}_i^{\mathrm{T}} + \tilde{\boldsymbol{R}}_{k,i})/b_{k,i}^2, \tag{10}$$

$$\boldsymbol{\psi}_{k,i} \leftarrow \boldsymbol{\psi}_{k,i} + \boldsymbol{P}_{k,i} \boldsymbol{H}^{\mathrm{T}} \boldsymbol{R}_{\mathrm{x}}^{-1} (\bar{\boldsymbol{z}}_{k,i} - \boldsymbol{H} \boldsymbol{\psi}_{k,i}), \tag{11}$$

$$\boldsymbol{P}_{k,i|i} \leftarrow \boldsymbol{P}_{k,i} - \boldsymbol{P}_{k,i} \boldsymbol{H}^{\mathrm{T}} \boldsymbol{R}_{\mathrm{x}}^{-1} \boldsymbol{H} \boldsymbol{P}_{k,i}, \tag{12}$$

where "$\leftarrow$" denotes the sequential assignment [12]. In light of the measurement model (6) and (5), the autocorrelation matrix $\boldsymbol{R}_{\mathrm{x}}$ of the innovation process can be readily obtained in (10) with $\tilde{\boldsymbol{R}}_{k,i} = \sum_{l \in \mathcal{V}_k} n_{l,i} \boldsymbol{R}_{l,i}$. The matrices $\hat{\boldsymbol{\Omega}}_i$ and $\hat{\boldsymbol{L}}_i$ in (10) are calculated with the entries of the estimate $\hat{\boldsymbol{e}}_{k,i|i-1} = [\hat{a}_{k,i|i-1}^1, \hat{a}_{k,i|i-1}^2, \hat{\theta}_{k,i|i-1}]^{\mathrm{T}}$ of $\boldsymbol{e}_i$ in light of (2) [12], [17]. Whereas $\hat{\boldsymbol{e}}_{k,i|i-1}$ is obtained in (33) presented further ahead.

2) Extension State: We consider herein that each node k would independently estimate the shape parameters at each time instant i, including the semi-axes $a_{1,i}$, $a_{2,i}$ and the orientation θ_i, and then utilize the extension matrix $\boldsymbol{S}_i$ for data combination in Sec. III-B.

We first consider the estimation of the semi-axes. Following [17], we estimate each semi-axis $a_{t,i}$ of the object by constructing the pseudo-measurement $q_{k,i}^t$, which refers to a measurement of the semi-axis. Specifically, the intermediate estimate $\phi_{k,i}^t$ and the corresponding error covariance $B_{k,i}^t$ of each semi-axis $a_{t,i}$ would be updated at each node k via the Kalman filter as follows:

$$\phi_{k,i}^t \leftarrow \hat{a}_{k,i|i-1}^t, \tag{13}$$
$$B_{k,i|i}^t \leftarrow B_{k,i|i-1}^t, \tag{14}$$
$$g_{\mathrm{a}} \leftarrow B_{k,i|i}^t + \upsilon_{k,i}^t, \tag{15}$$
$$\phi_{k,i}^t \leftarrow \phi_{k,i}^t + B_{k,i|i}^t g_{\mathrm{a}}^{-1}(q_{k,i}^t - \phi_{k,i}^t), \tag{16}$$
$$B_{k,i|i}^t \leftarrow B_{k,i|i}^t - B_{k,i|i}^t g_{\mathrm{a}}^{-1} B_{k,i|i}^t, \tag{17}$$

where $\hat{a}_{k,i|i-1}^t$ denotes $i-1$ instant predicted value of the semi-axis $a_{t,i-1}$, $B_{k,i|i-1}^{\mathrm{t}}$ represents the (t,t)th entry of $\boldsymbol{B}_{k,i|i-1}$, which is obtained in (33) presented further ahead. The variance $\upsilon_{k,i}^t$ of the pseudo-measurement $q_{k,i}^t$ is given in (27).

In light of (5), the sample covariance matrix of the measurements can be expressed as follows

$$\bar{\boldsymbol{Z}}_{k,i} \triangleq \frac{1}{b_{k,i}-1} \sum\nolimits_{\iota=1}^{b_{k,i}} \left(\boldsymbol{z}_{k,i}^{(\iota)} - \bar{\boldsymbol{z}}_{k,i}\right)\left(\boldsymbol{z}_{k,i}^{(\iota)} - \bar{\boldsymbol{z}}_{k,i}\right)^{\mathrm{T}}. \tag{18}$$

with the measurement average $\bar{\boldsymbol{z}}_{k,i}$. Note that the second-order moment $\bar{\boldsymbol{Z}}_{k,i}$ could be constructed with the measurements. The orientation and semi-axes of the extended object could be extracted with the eigenvalue decomposition of $\bar{\boldsymbol{Z}}_{k,i}$ [22].

According to (6) and (5), each measurement of each neighboring node $\boldsymbol{z}_{k,i}^{(\iota)}$ is Gaussian distributed [5]. Consequently, $\bar{\boldsymbol{Z}}_{k,i}$ follows the Wishart distribution with $b_{k,i}-1$ degrees of freedom [23], [24]

$$\bar{\boldsymbol{Z}}_{k,i} \sim \mathcal{W}\left(b_{k,i}-1,\ \frac{\omega b_{k,i}\boldsymbol{\Omega}_i \boldsymbol{L}_i^2 \boldsymbol{\Omega}_i^{\mathrm{T}} + \tilde{\boldsymbol{R}}_{k,i}}{(b_{k,i}-1)^2}\right). \tag{19}$$

To proceed, the eigenvalue decomposition of $\tilde{\boldsymbol{Z}}_{k,i} \triangleq \frac{b_{k,i}-1}{\omega b_{k,i}}\bar{\boldsymbol{Z}}_{k,i}$ is given by $\tilde{\boldsymbol{Z}}_{k,i} = \boldsymbol{U}_{k,i}\boldsymbol{\Lambda}_{k,i}\boldsymbol{U}_{k,i}^{\mathrm{T}}$, where the columns of $\boldsymbol{U}_{k,i}$ are the eigenvectors of $\tilde{\boldsymbol{Z}}_{k,i}$, and $\boldsymbol{\Lambda}_{k,i}$ is the diagonal matrix containing the corresponding eigenvalues,

$$\boldsymbol{U}_{k,i} \triangleq \begin{bmatrix} u_{11} & u_{12} \\ u_{21} & u_{22} \end{bmatrix}, \quad \boldsymbol{\Lambda}_{k,i} \triangleq \begin{bmatrix} \lambda_1 & 0 \\ 0 & \lambda_2 \end{bmatrix}. \tag{20}$$

Since $(b_{k,i}-1)/(\omega b_{k,i})$ is positive and the matrix $\boldsymbol{U}_{k,i}$ is non-singular, utilizing the properties of the Wishart distribution [23], [24], we can deduce that $\boldsymbol{\Lambda}_{k,i}$ also follows the Wishart distribution,

$$\boldsymbol{\Lambda}_{\boldsymbol{k,i}} \sim \mathcal{W}\left(b_{k,i}-1,\ \frac{\boldsymbol{U}_{k,i}^{\mathrm{T}}\boldsymbol{\Omega}_i \boldsymbol{L}_i^2 \boldsymbol{\Omega}_i^{\mathrm{T}} \boldsymbol{U}_{k,i} + \boldsymbol{W}_{k,i}}{b_{k,i}-1}\right), \tag{21}$$

with

$$\boldsymbol{W}_{k,i} \triangleq \frac{1}{\omega b_{k,i}} \boldsymbol{U}_{k,i}^{\mathrm{T}} \tilde{\boldsymbol{R}}_{k,i} \boldsymbol{U}_{k,i} = \begin{bmatrix} w_1 & * \\ * & w_2 \end{bmatrix}. \tag{22}$$

where $*$ indicates the irrelevant values. According to [17], the expectation of $\boldsymbol{U}_{k,i}$ is given by $\boldsymbol{\Omega}_i$. Accordingly, we have $\boldsymbol{U}_{k,i}^{\mathrm{T}}\boldsymbol{\Omega}_i \approx \boldsymbol{I}_2$, as $\boldsymbol{\Omega}_i$ could be approximated by $\boldsymbol{U}_{k,i}$. Thus, (21) can be rewritten as

$$\boldsymbol{\Lambda}_{k,i} \sim \mathcal{W}\left(b_{k,i}-1,\ \frac{\boldsymbol{L}_i^2 + \boldsymbol{W}_{k,i}}{b_{k,i}-1}\right). \tag{23}$$

Accordingly, based on the marginal distribution properties of the Wishart distribution [23], each eigenvalue λ_t in $\boldsymbol{\Lambda}_{k,i}$ follows the Gamma distribution [23]

$$\lambda_t \sim \Gamma\left(\frac{b_{k,i}-1}{2},\ \frac{2(a_{t,i}^2 + w_t)}{b_{k,i}-1}\right),\ \ t=1,2, \tag{24}$$

where $\Gamma(\alpha,\beta)$ denotes the Gamma distribution with the shape parameter α and scale parameter β.

It is noteworthy that the expectation of each diagonal entry of $\boldsymbol{\Lambda}_{k,i} - \boldsymbol{W}_{k,i}$ corresponds to the square of the semi-axis $a_{t,i}^2$. To facilitate the subsequent derivation, we introduce

$$(q_{k,i}^t)^2 \triangleq \lambda_t - w_t,\ \ t=1,2. \tag{25}$$

Leveraging the second-order moment matching [17] and the delta method [25], we approximate the distribution of $q_{k,i}^t$ by the following Gaussian distribution

$$q_{k,i}^t \sim \mathcal{N}\left(a_{t,i},\ \upsilon_{k,i}^t\right),\ \ t=1,2, \tag{26}$$

with

$$\upsilon_{k,i}^t = ((q_{k,i}^t)^2 + w_t)/(2(q_{k,i}^t)^2(b_{k,i}-1)). \tag{27}$$

Next, we consider the localized adaptation of the orientation

$$\mathcal{S}_{k,i} = \mathcal{S}_{k,i}^{\mathrm{eig}} \tag{28}$$

where $\mathcal{S}^{\mathrm{eig}}$ is calculated from (1), $\boldsymbol{\Omega}_i$ and $\boldsymbol{L}_i$ in (1) are derived from (2) using the shape parameters $[\phi_{k,i}^1, \phi_{k,i}^2, \phi_{k,i}^{\mathrm{eig}}]^{\mathrm{T}}$.

By approximating $\boldsymbol{\Omega}_i$ with $\boldsymbol{U}_{k,i}$, we could use $\boldsymbol{U}_{k,i}$ to compute the orientation. At each time instant i, each node k would determine the orientation using the eigenvector-based estimate

$$\phi_{k,i}^{\mathrm{eig}} = \mathrm{atan2}\left(u_{21}, u_{11}\right) \tag{29}$$

where $\mathrm{atan2}(\cdot)$ denotes the four-quadrant arcus tangent function, u_{21} and u_{11} are the elements of the first column of the eigenvector matrix in (20).

B. Combination

We now consider the combination at each node k to enhance the comprehensive tracking performance. Specifically, akin to the ATC scheme of the diffusion strategy [6], [26], each node k would update its local estimates by respectively combing the intermediate kinematic $\boldsymbol{\psi}_{l,i}$ and extension $\mathcal{S}_{l,i}$ of the object shared by each neighboring node $l \in \mathcal{V}_k$,

$$\hat{\boldsymbol{x}}_{k,i|i} = \sum\nolimits_{l\in\mathcal{V}_k} c_{lk,i}\boldsymbol{\psi}_{l,i}, \quad \hat{\boldsymbol{S}}_{k,i|i} = \sum\nolimits_{l\in\mathcal{V}_k} c_{lk,i}\mathcal{S}_{l,i}, \tag{30}$$

with the nonnegative weight $c_{lk,i}$ satisfying $\sum_{l\in\mathcal{V}_k} c_{lk,i} = 1$ [6], [10], [26].

Subsequently, each entry of the local estimate of the shape vector $\hat{\boldsymbol{e}}_{k,i|i} = [\hat{a}^1_{k,i|i}, \hat{a}^2_{k,i|i}, \hat{\theta}_{k,i|i}]^{\mathrm{T}}$ is given by the eigenvalue decomposition on the local estimate of the extension matrix $\hat{\boldsymbol{S}}_{k,i|i}$

$$\hat{a}^1_{k,i|i} = \sqrt{\vartheta^1_{k,i}}, \quad \hat{a}^2_{k,i|i} = \sqrt{\vartheta^2_{k,i}}, \quad \hat{\theta}_{k,i|i} = \operatorname{atan2}\left(\nu_{21}, \nu_{11}\right), \tag{31}$$

where $\vartheta^1_{k,i}$ and $\vartheta^2_{k,i}$ are the eigenvalues, and $[\nu^1_{k,i}, \nu^2_{k,i}]^{\mathrm{T}}$ is the principal eigenvector of $\hat{\boldsymbol{S}}_{k,i|i}$.

C. Time-update

As the temporal evolution of the state of the object in (3) follows the linear model, the time update of the kinematic and extension states of each node k is given by

$$\begin{aligned} \hat{\boldsymbol{x}}_{k,i+1|i} &= \boldsymbol{F}^{\mathrm{x}}_i \hat{\boldsymbol{x}}_{k,i|i}, \\ \boldsymbol{P}_{k,i+1|i} &= \boldsymbol{F}^{\mathrm{x}}_i \boldsymbol{P}_{k,i|i} \left(\boldsymbol{F}^{\mathrm{x}}_i\right)^{\mathrm{T}} + \boldsymbol{Q}^{\mathrm{x}}_i, \end{aligned} \tag{32}$$

and

$$\begin{aligned} \hat{\boldsymbol{e}}_{k,i+1|i} &= \boldsymbol{F}^{\mathrm{e}}_i \hat{\boldsymbol{e}}_{k,i|i}, \\ \boldsymbol{B}_{k,i+1|i} &= \boldsymbol{F}^{\mathrm{e}}_i \boldsymbol{B}_{k,i|i} \left(\boldsymbol{F}^{\mathrm{e}}_i\right)^{\mathrm{T}} + \boldsymbol{Q}^{\mathrm{e}}_i. \end{aligned} \tag{33}$$

The implementation of the proposed RDEOT algorithm is summarized in Algorithm 1. It is noteworthy that the DRM [11] involves multiple matrix square root operations, whereas the DEOKF algorithm [12] requires sequential iterations to update the local estimate. In contrast, our proposed DEOT algorithm avoids these computational burdens, resulting in significantly improved efficiency.

D. Complexity Analysis

We now evaluate the computational complexity of the proposed distributed algorithms in terms of real-valued multiplications at each node k per iteration [6]. For brevity, we assume that the number $n_{k,i}$ of the measurements obtained at each node k at each time instant i is the same. Let d_k denote the number of neighbors of each node k.

TABLE I
THE COMPUTATIONAL COMPLEXITY.

Algorithm	Computational Complexity
DRM [11]	$39d_k + 4n_{k,i} + 1022$
DEOKF [12]	$7d_k + 563n_{k,i} + 207$
DEOT	$10d_k + 4d_k n_{k,i} + 518$

As summarized in Table I, the computational complexity of the proposed DEOT algorithm is significantly lower than that of both DRM [11] and DEOKF [12], particularly in scenarios with a large number of measurements $n_{k,i}$. This reduction in computational overhead makes DEOT well-suited for resource-constrained distributed networks.

Algorithm 1: DEOT

Initialize: For each node k, initialize $\hat{\boldsymbol{x}}_{k,0|-1}$, $\boldsymbol{P}_{k,0|-1}$, $\hat{\boldsymbol{e}}_{k,0|-1}$, $\boldsymbol{B}_{k,0|-1}$.
At each time step $i > 0$**:**
for *each node* k **do**
  1: Localized Adaptation
  Update the intermediate estimates $\boldsymbol{\psi}_{k,i}$ and $\boldsymbol{P}_{k,i}$ of the kinematic state via (8)-(12).
  Calculate the pseudo-measurements $q^t_{k,i}$ of the semi-axis through (26).
  Update the intermediate estimates $\phi^t_{k,i}$ and $\boldsymbol{B}^t_{k,i}$ of the semi-axis via (13)-(17).
  Update the intermediate estimate $\phi^{\mathrm{eig}}_{k,i}$ of the orientation via (29).
  Calculate the intermediate estimates $\boldsymbol{\chi}_{k,i}$ of the extension matrix.
  2: Combination
  Exchange $\boldsymbol{\psi}_{k,i}$ and $\boldsymbol{\chi}_{k,i}$ with $l \in \mathcal{N}_k$.
  Update the local estimates via (30).
  Decompose the shape parameters using (31).
  3: Time-update
  Update the pre-estimate via (32) and (33).

IV. SIMULATION RESULTS

We herein evaluate the tracking performance of proposed DEOT, the distributed extended object tracking (DRM), and the distributed extended object tracking (DEOKF).

We consider tracking a single extended object modeled as an ellipse with the major and minor axes of 340 m and 80 m [5], [12], [15], with an adaptive network of $N = 25$ nodes. The object is initially located at $\boldsymbol{\rho}_0 = [0, 0]^{\mathrm{T}}$ m, and moves at a constant speed of 27 knots along with a series of turns. The network topology as well as the ground truth trajectory are illustrated in Fig. 3(a).

Following [5], [12], [15], we consider that the shape and size of the object would remain constant during the maneuvering. Accordingly, the process matrices are respectively given by

$$\boldsymbol{F}^{\mathrm{x}}_i = \begin{bmatrix} \boldsymbol{I}_2 & T\boldsymbol{I}_2 \\ \boldsymbol{O}_2 & \boldsymbol{I}_2 \end{bmatrix}, \quad \boldsymbol{F}^{\mathrm{e}}_i = \boldsymbol{I}_3,$$

with the sampling interval $T = 10$ s. The process noise covariance matrices of the kinematic and extension states of the object are set to be $\boldsymbol{Q}^{\mathrm{x}}_i = \mathrm{diag}\{100, 100, 1, 1\}$ and $\boldsymbol{Q}^{\mathrm{e}}_i = \mathrm{diag}\{10, 10, 0.1\}$, respectively. The fluctuant number $n_{k,i}$ of local measurements at each node k per time instant follows the Poisson distribution with the mean 20 [5], [15]. The constant associated with the additive noise is $\xi = 1\times10^{-5}$. In addition, the priors for the kinematic and extension states of each node k are set to be $\hat{\boldsymbol{x}}_{k,0|-1} = [50, 50, 10, -10]^{\mathrm{T}}$, $\boldsymbol{P}_{k,0|-1} = \mathrm{diag}\{900\boldsymbol{I}_2, 16\boldsymbol{I}_2\}$, $\hat{\boldsymbol{e}}_{k,0|-1} = [140, 90, -\pi/3]^{\mathrm{T}}$ and $\boldsymbol{B}_{k,0|-1} = \mathrm{diag}\{70^2, 70^2, 1\}$.

We use the Gaussian Wasserstein Distance (GWD) [3], [4], which comprehensively describes the extended object

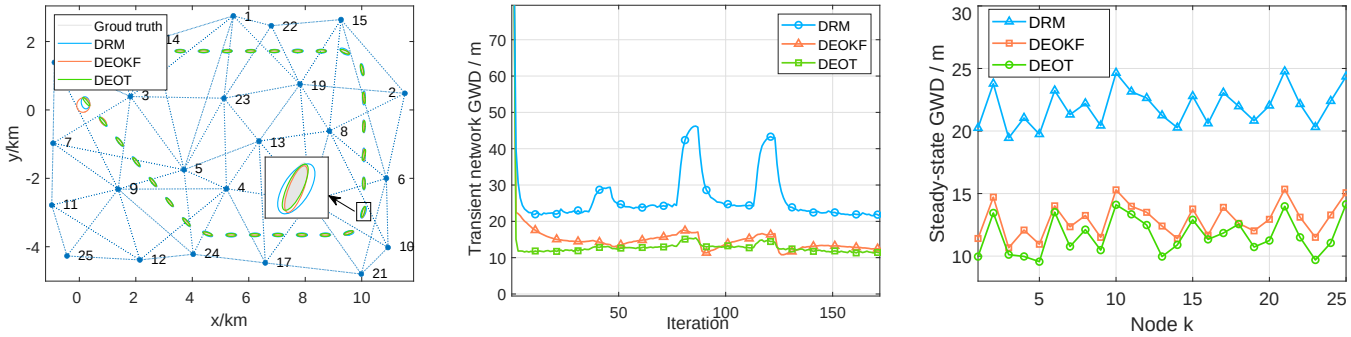

(a) (b) (c)

Fig. 3. Comprehensive performance comparison. (a) Measurements, trajectory, and estimation results. (b) Transient GWD performance of different algorithms. (c) Steady-state GWD performance of different algorithms.

tracking performance, as the performance evaluation metric. Specifically, at each time instant i, the GWD at each node k in the adaptive network is defined as

$$\mathrm{GWD}_{k,i} \triangleq \frac{1}{J}\sum_{\zeta=1}^{J}\sqrt{\mathrm{GWD}_{k,i}^{2}(\zeta)}, \tag{34}$$

with

$$\begin{aligned}\mathrm{GWD}_{k,i}^{2}(\zeta) &\triangleq \left\|\boldsymbol{x}_i - \hat{\boldsymbol{x}}_{k,i|i}(\zeta)\right\|^2 \\ &+ \mathrm{tr}\left\{\boldsymbol{S}_i + \hat{\boldsymbol{S}}_{k,i|i}(\zeta) - 2\sqrt{\sqrt{\boldsymbol{S}_i}\hat{\boldsymbol{S}}_{k,i|i}(\zeta)\sqrt{\boldsymbol{S}_i}}\right\},\end{aligned} \tag{35}$$

where $\hat{\boldsymbol{x}}_{k,i|i}(\zeta)$ and $\hat{\boldsymbol{S}}_{k,i|i}(\zeta)$ denote the instantaneous estimates of the kinematic state $\boldsymbol{x}_i$ and the extension matrix $\boldsymbol{S}_i$ at each node k in the ζth trial. The transient network GWD is defined as $\mathrm{GWD}_i^{\mathrm{net}} \triangleq \frac{1}{N}\sum_{k=1}^{N}\mathrm{GWD}_{k,i}$. The steady-state nodal and network GWDs are obtained by averaging the corresponding transient GWDs over 50 iterations after convergence, respectively. All the simulation results are averaged over $J = 500$ independent trials.

We herein evaluate the performance of the different algorithms. The trajectory estimates of the elliptical object in a typical trial and the comprehensive tracking performance of different algorithms are presented in Figs. 3, respectively.

It can be observed that the proposed DEOT algorithm outperforms its competitors, attributed to the characterization of the object extension with both the shape parameter vector and the extension matrix, especially when the object undergoes turning maneuvers. In contrast, the comprehensive tracking performance of the DRM remarkably deteriorates at each turn of the object.

Moreover, it can be observed in Table II that the proposed DEOT algorithm is computationally more efficient than the competitors. In contrast, the DEOKF sequentially iterates over each measurement for localized adaptation, resulting in a marked increase in computational burden.

V. Conclusions

We develop a distributed extended object tracking algorithm for an adaptive network based on the adapt-then-combine scheme of the diffusion strategy. Specifically, we improve computational efficiency by designing the algorithm to simultaneously process multiple measurements at each node. The simulation results validate the superior performance as well as the computational efficiency of the proposed DEOT algorithm for adaptive networks.

TABLE II
Ratio of calculation time to the baseline DRM [11] algorithm

Algorithm	DEOKF [12]	DEOT
Relative Runtime	2.22	0.52

References

[1] M. Hurtado, J.-J. Xiao, and A. Nehorai, "Target estimation, detection, and tracking," *IEEE Signal Processing Mag.*, vol. 26, no. 1, pp. 42–52, 2009.

[2] L. Sun, H. Yu, Z. Fu, Z. He, and J. Zou, "Modeling and tracking of maneuvering extended object with random hypersurface," *IEEE Sens. J.*, vol. 21, no. 18, pp. 20 552–20 562, 2021.

[3] K. Granstrom, M. Baum, and S. Reuter, "Extended object tracking: Introduction, overview and applications," *J. Adv. Inf. Fusion*, vol. 12, no. 2, pp. 139–174, 2017.

[4] K. Granström and M. Baum, "A tutorial on multiple extended object tracking," *Authorea Preprints*, 2023. DOI: 10.36227/techrxiv.19115858.v1.

[5] S. Yang and M. Baum, "Tracking the orientation and axes lengths of an elliptical extended object," *IEEE Trans. Signal Process.*, vol. 67, no. 18, pp. 4720–4729, 2019.

[6] F. S. Cattivelli and A. H. Sayed, "Diffusion strategies for distributed Kalman filtering and smoothing," *IEEE Trans. Automat. Contr.*, vol. 55, no. 9, pp. 2069–2084, 2010.

[7] A. H. Sayed, "Adaptive networks," *Proc. of the IEEE*, vol. 102, no. 4, pp. 460–497, 2014.

[8] Z. Li, Y. Liang, and L. Xu, "Distributed extended object tracking using coupled velocity model from WLS perspective," *IEEE Trans. Signal Inform. Process. over Netw.*, vol. 8, pp. 459–474, 2022.

[9] J. Lou, L. Jia, R. Tao, and Y. Wang, "Distributed incremental bias-compensated rls estimation over multi-agent networks," *Sci. China Inf. Sci.*, vol. 3, no. 60, pp. 1–15, 2017.

[10] A. H. Sayed, "Diffusion adaptation over networks," in *Academic Press Library in Signal Processing*, vol. 3, Elsevier, 2014, pp. 323–453.

[11] W. Li, Y. Jia, D. Meng, and J. Du, "Distributed tracking of extended targets using random matrices," in *Proc. IEEE Conf. Decis. Control*, Osaka, Japan, 2015, pp. 3044–3049.

[12] Y. Ren and W. Xia, "Distributed extended object tracking based on diffusion strategy," in *Proc. 28th European Signal Process. Conf.*, Amsterdam, Netherlands, 2021, pp. 2338–2342.

[13] J. W. Koch, "Bayesian approach to extended object and cluster tracking using random matrices," *IEEE Trans. Aerosp. Electron. Syst.*, vol. 44, no. 3, pp. 1042–1059, 2008.

[14] J. Liu and G. Guo, "Distributed asynchronous extended target tracking using random matrix," *IEEE Sensors J.*, vol. 20, no. 2, pp. 947–956, 2020.

[15] J. Lan and X. R. Li, "Tracking of extended object or target group using random matrix: New model and approach," *IEEE Trans. Aerosp. Electron. Syst.*, vol. 52, no. 6, pp. 2973–2989, 2016.

[16] B. Tuncer and E. Özkan, "Random matrix based extended target tracking with orientation: A new model and inference," *IEEE Trans. Signal Process.*, vol. 69, pp. 1910–1923, 2021.

[17] F. Govaers, "On independent axes estimation for extended target tracking," in *Proc. IEEE Sens. Data Fusion: Trends Solut. Appl.*, Bonn, Germany, 2019, pp. 1–6.

[18] W. Xia and Y. Zhang, "Resilient distributed estimation against FDI attacks: A correntropy-based approach," *Information Sciences*, vol. 635, pp. 236–256, 2023.

[19] Q. Shi, M. Feng, X. Li, S. Wang, and F. Chen, "A secure distributed information sharing algorithm based on attack detection in multi-task networks," *Transactions on Circuits and Systems I: Regular Papers*, vol. 67, no. 12, pp. 5125–5138, 2020.

[20] M. Feldmann, D. Fränken, and W. Koch, "Tracking of extended objects and group targets using random matrices," *IEEE Trans. Signal Process.*, vol. 59, no. 4, pp. 1409–1420, 2011.

[21] W. Xia, Z. Zhou, W. Jiang, and Y. Zhang, "Dynamic UAV swarm confrontation: An imitation based on mobile adaptive networks," *IEEE Trans. Aerosp. Electron. Syst.*, vol. 59, no. 5, pp. 7183–7202, 2023.

[22] F. Husson, S. Lê, and J. Pagès, "Confidence ellipse for the sensory profiles obtained by principal component analysis," *Food Quality and Preference*, vol. 16, no. 3, pp. 245–250, 2005.

[23] F. Edition, A. Papoulis, and S. U. Pillai, *Probability, random variables, and stochastic processes*. New York, NY, USA: McGraw-Hill Europe, 2002.

[24] A. K. Gupta and D. K. Nagar, *Matrix variate distributions*. New York, NY, USA: Chapman and Hall/CRC, 2018.

[25] G. W. Oehlert, "A note on the delta method," *The American Statistician*, vol. 46, no. 1, pp. 27–29, 1992.

[26] F. S. Cattivelli and A. H. Sayed, "Diffusion LMS strategies for distributed estimation," *IEEE Trans. Signal Process.*, vol. 58, no. 3, pp. 1035–1048, 2010.